Advances in Natural Sciences:
Nanoscience and Nanotechnology

Development of a fluorescent label tool based on lanthanide nanophosphors for viral biomedical application

OPEN ACCESS
IOP PUBLISHING ADVANCES IN NATURAL SCIENCES: NANOSCIENCE AND NANOTECHNOLOGY
Adv. Nat. Sci.: Nanosci. Nanotechnol. **3** (2012) 035003 (10pp) doi:10.1088/2043-6262/3/3/035003

Development of a fluorescent label tool based on lanthanide nanophosphors for viral biomedical application

Quoc Minh Le[1,2], Thu Huong Tran[1], Thanh Huong Nguyen[1], Thi Khuyen Hoang[1], Thanh Binh Nguyen[1], Khanh Tung Do[1], Kim Anh Tran[1], Dang Hien Nguyen[3], Thi Luan Le[3], Thi Quy Nguyen[3], Mai Dung Dang[3], Nu Anh Thu Nguyen[3] and Van Man Nguyen[3]

[1] Institute of Materials Science, Vietnam Academy of Science and Technology, 18 Hoang Quoc Viet, Cau Giay, Hanoi, Vietnam
[2] University of Engineering and Technology, Vietnam University Hanoi, Xuan Thuy, Cau Giay, Hanoi, Vietnam
[3] Center for Research and Production of Vaccines and Biologicals, Vietnam Ministry of Health, 135 Lo Duc, Hai Ba Trung, Hanoi, Vietnam

E-mail: lequocminh@ims.vast.ac.vn

Received 9 April 2012
Accepted for publication 12 April 2012
Published 29 May 2012
Online at stacks.iop.org/ANSN/3/035003

Abstract

We report for the first time the preparation of luminescent lanthanide nanomaterial (LLN) linked bioconjugates and their application as a label tool for recognizing virus in the processing line of vaccine industrial fabrication. Several LLNs with the nanostructure forms of particles or rods/wires with europium (III) and terbium (III) ions in lattices of vanadate, phosphate and metal organic complex were prepared to develop novel fluorescent conjugates able to be applied as labels in fluorescence immunoassay analysis of virus/vaccine.

With regard to the LLNs, we have successfully synthesized nanoparticles around 10 nm of YVO_4 : Eu(III), with high emission in the red spectral region, nanorod and nanowire of $TbPO_4 \cdot H_2O$ and $Eu_{1-x}Tb_xPO_4 \cdot H_2O$, width 5–7 nm and length 300 nm, showing very bright luminescence in green, and core/shell nanosized Eu(III) and Tb(III)/Eu(III) complexes with naphthoyl trifluoroacetone and tri-*n*-octylphosphineoxide (Eu.NTA.TOPO@PVP, Eu_XTb_{1-X}.NTA.TOPO). The appropriated core/shell structures can play a double role, one for enhancing luminescence efficiency and another for providing nanophosphors with better stability in water media for facilitating the penetration of nanophosphor core into a biomedical environment.

The organic functionalizations of the obtained LLNs were done through their surface encapsulation with a functional polysiloxane including active groups such as amine (NH_2), thiocyanate (SCN) or mecarpto (SH). The properties of functional sol-gel matrix have great influence on the luminescence properties, especially luminescence intensity of YVO_4 : Eu(III), Eu.NTA.TOPO@PVP, $TbPO_4 \cdot H_2O$ and $Eu_xTb_{1-x}PO_4 \cdot H_2O$. Bioconjugation processes of the functionalized LLNs have been studied with some bioactive molecules such as biotin, protein immunoglobulin G (IgG) or bovine serum albumin (BSA).

The results of LLN-bioconjugate linking with IgG for recognizing virus (vaccine) will be presented in brief. It is consistent to state that the LLN bioconjugates prepared from YVO_4 : Eu(III)–nanoparticles, $TbPO_4 \cdot H_2O$ nanorod or wire and EuNTA.TOPO@PVP nanosized core/shell complex could be used as labels for recognizing virus in diagnosis or in vaccine production by use of the fluorescence immunoassay (FIA) method. The fluorescence images of the incubated specimens consisting of LLN bioconjugate and vaccine fabricate could be obtained well in terms of sharpness, reproductivity and stability.

However, much work still needs to be done to develop an ordinary LLN-conjugate using the FIA method for analysis of virus and, moreover, to extend the study of biomedical cell processes at nano/microscale in practical application.

Keywords: nanoparticles, functionalization, conjugation, label, fluorescence immunoassay, vaccine

Classification numbers: 2.05, 4.03, 4.06, 4.07

1. Background

Nanophotonics broadly impacts biomedical research and engineering for studying fundamental interactions and dynamics at single cell/molecule level, as well as for light-guided detection and light-activated therapy in nanomedicine. Nanomedicine is an emerging field that deals with utilization of nanomaterials in the development of new methods of minimally invasive diagnostics for early detection and recognition of diseases, as well as for facilitating and real-time monitoring of drug-vaccine action.

Among the nanomaterials luminescent ones become increasingly more effective biomedical tools [1], especially for labeling in diagnosis [2] and cell imaging [3]. Development and potential application of nanotechnology tools for biomolecules, cell and especially virus detection by emergent photonic nanotechnology are likely to revolutionize diagnosis and to determine treatment endpoints for life-threatening virus infections [4]. Virus particles are natural nanomaterials and have received particular attention as novel building blocks for designing, elucidating and determining. Medical diagnostics, especially in the field of clinical virology, significantly depends on detection of viral antigen, virus particles or genomic materials in samples from infected individuals. The visualization, characterization and quantification of biological processes at the molecular and cellular levels in humans and other organisms are the vast and most critical applications of nanotechnology in viral biology and infected disease medicine [5].

The introduction of labeling agents into biological viral systems is usually required as an organism lacks sensitive detectable signals. Biological analysis was first introduced by American scientists Yalow and Benson in the form of radioimmunoassay (RIA) [6]. Although there are many advantages in using RIA, owing to its high sensitivity and wide application, it does have a number of drawbacks, such as its radioactivity and inherently short half life [7]. Therefore, various nonradiative labeling techniques based on enzyme-catalyzed reactions, bio/chemiluminescence's and fluorescence, for example, have emerged, among which fluorescent labeling is the most widely used [8,9]. Organic dyes are amongst the earliest types of classical fluorescent labels used in biology. Despite their inherent drawbacks such as having a short Stockes shift, poor photochemical stability, susceptibility to photobleaching and decomposition under repeated excitation, organic dyes are still popular due to their low cost, availability and ease of usage [10]. Recently quantum dots (QDs), semiconductor nanocrystals composed of atoms from groups II–VI or III–V of the periodic

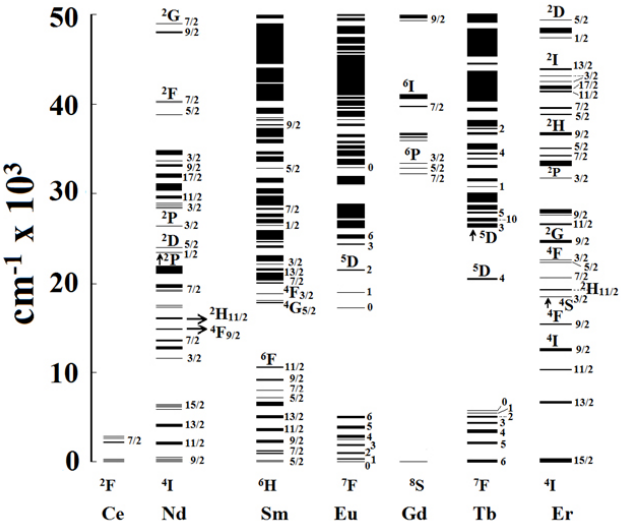

Figure 1. Energy level of the $4F_n$ configuration of luminescent trivalent lanthanide ions.

table, show unique optical properties making them appealing as fluorescent labels in biological investigations. However, despite QDs' potential and success so far in biological applications, there exist several limitations associated with their use. A typical problem with QDs is optical blinking, which makes the application of QDs in qualitative assays difficult. Furthermore, QDs themselves are not biocompatible and have to be surface modified before they are used in live cell or animal experiments. In regards to sustainable development, QDs have great problems with toxicity of the heavy metals they are fabricated from [11].

On the other hand, like semiconductor-based luminescent materials, conventional lanthanide-doped bulk phosphors have played a vital role in numerous practical applications such as laser, monitor screen, fluorescent lamp and display. The energy flow in the lanthanide compound is derived by the transition from excited singlet level through intersystem crossing to triplet state and from this triplet state to the imitative levels of the lanthanide ion. Figure 1 shows a simplified diagram of the relevant energy levels of various luminescent lanthanides. Among the lanthanides there are two elements, Eu and Tb, with strong emission potential in red or green spectral regions, as the most attractive tools for biomedical labeling or imaging.

However, studies on nanoparticles of these materials are largely behind those of quantum dots. Increasingly, efforts have been focused on lanthanide-doped luminescent nanoparticles and this has yielded notable progress. Several research groups have reported the synthesis of well

dispersed colloids of yttrium vanadate and lanthanum fluoride nanoparticles doped with lanthanide (III) [12–15].

Especially, the approach for synthesis of the core/shell nanoparticles, in which the core is doped with luminescent lanthanide ion, has solved the problem of low quantum yield that is inherent to lanthanide-doped with lanthanide luminescent nanoparticles [16,17]. In particular, they are strongly fluorescent, less toxic and readily synthesized in water, which greatly facilitates further biofunctionalization. More recently, there was the first report on inorganic lanthanide phosphate fluorescent nanorods as fluorescent labels in human umbilical vein endothelical cells (HUVEC), 760-O cells [12] in live cell biology [18] and later on functionalized europium hydroxide nanorods for *in vitro* imaging of human lung carcinoma cells [19]. Indeed lanthanide orthophosphate ($LnPO_4$) belongs to two polymorphic types, the monoclinic monazite type (for La to Gd) and quadratic xenotime type (for Tb to Lu). Due to high quantum efficiency (QE), bulk lanthanide phosphate as an ideal host in fluorescent lamps, cathode ray type (CRT) and plasma display panel (PDP), has been extensively investigated. It is expected that nanosized rare earth (RE) compounds can increase luminescent QE and display resolution. To improve luminescent properties of nanocrystalline phosphors, many preparation methods have been used such as solid state reactions, sol–gel techniques, hydroxide preparation, and hydrothermal synthesis, spray pyrolysis, laser-heated evaporation, combustion synthesis with the assistance of ultrasound and microwave. Currently, the luminescent RE-doped low dimensional nanomaterials such as $LaPO_4$ nanowires [20], $Y_2O_3:RE$ and $La_2O_3:Eu$ nanotubes/nanowires [21] are also attracting considerable interest. One-dimensional 1D and 2D structures, such as tubes, wires, rods and belts, have aroused remarkable attention over the past decade due to a great deal of potential applications, such as data storage [22], advanced catalyst [23] and photoelectronic devices [24]. On the other hand, in comparison with 0D structures, the space anisotropy of 1D structures provides a better model system to study the dependence of electronic transport and optical and mechanical properties on size confinement and dimensionality [25]. Therefore, it is expected that the effect of 0D and 1D nanomaterials based on lanthanide luminescent nanocrystals will clearly happen in the field of biology and medicine.

Despite the above attractive features, the forbidden nature of $^4f_5$–$^4f_5$ transition of lanthanide ions has nevertheless limited the brightness of lanthanide-based biolabels for cell and virus imaging. Antenna-lanthanide ion energy transfer is an effective way to improve the quantum efficiency of lanthanide materials [26]. As a matter of fact, lanthanide-based nanomaterials are stable and are easy to fabricate and functionalize. The lanthanide nanophosphors can readily be internalized by cells and generally exhibit no apparent detrimental effect on cell viability. Thus, besides biolabeling, they are also good candidates for *in vitro* and *in vivo* targeted drug/gene delivery vehicles. Nevertheless, most nanoparticles reported in past immunoassays are >30 nm in diameter. These particles sizes are proven to bring obvious prolonged equilibration time and enhanced nonspecific adsorption [27]. Therefore nanoparticles have a smaller size, their kinetic properties could meanwhile be improved and nonspecific adsorption decreased. Moreover, the nanoparticles should be big enough to bind several proteins on the surface, which is expected to increase the immunological affinity.

In the field of lanthanide luminescent nanomaterials, nanosized lanthanide chelates have a special position. The lanthanide chelate labels in biological studies contain typically organic chromospheres, which sensitize the absorption of the excitation light and the energy transfer to the lanthanide ions. Consequently, lanthanide chelates exhibit broad excitation spectra owing to the organic ligands and narrow emission spectra resulting from the lanthanide ions. Recently, their application to biological labeling has attracted growing interest due to their high photostability, quantum yield and good water solubility, and because they possess a reactive group that allows covalent attachment to the biomolecular system. The spectral characteristics include a long fluorescence lifetime (submicrosecond to millisecond range), sharply and spiky emission spectra, with full-width at half-maximum (FWHM) less than 10 nm, large stock shifts and high quantum yield [28].

Besides, rare earth upcoverting fluorescence nanophoshors have been developed as a novel generation of luminescent labels due to their super optical features in the near infrared spectral region from 800 to 1000 nm [29]. As this field is rapidly developing, we can expect that rare earth doped nanophosphors will find their way into even more elaborate biotechnological application in the future due to their relatively simple nanocomposition, deep penetration depth of near infrared (NIR) light and other advantageous photonic features [30,31].

In regards to developing a targeted biolabel, imaging tool, drug delivery and therapy, specific targeting functional groups on the surface of nanophosphors are desired to be conjugated to biomolecules, such as small molecules like biotin, avidine, streptavidin, macromolecules as peptides, antibodies or proteins. Apart from that, PEGylation, or linker incorporations on the surface may possibly be involved for certain labeling, imaging or therapy purposes. Once LLNs have been formed, an additional layer of linker molecules with various reactive functional groups (e.g. amine, thiol, thiocyanat or carboxyl) is often attached. These functional groups can act as a scaffold for the grafting of biological moieties by means of standard covalent bioconjugation schemes such as thioures coupling, base Schiff, thiol tag, amide forming and click chemistry [32] (figure 2). In addition to covalent binding to the LLNs' surface, bio-labeling entities can also be physically adsorbed onto the LLNs' surface using electrostatic interactions between LLNs and charged adapter molecules [33,34]. However, covalent binding of biomolecules to LLNs is preferred, not only to avoid desorbtion from the LLNs surface, but also to control the number and orientation of the immunobilized bi-recognition entities, which could be useable to develop a consistent tool for biomedical application.

To the best of our knowledge, there is no report on the study of LLNs (0D) and nanorod (1D) as a micro-optical fluorescent label for viral biomedical application. Based on these backgrounds the aim of our work is to develop a new

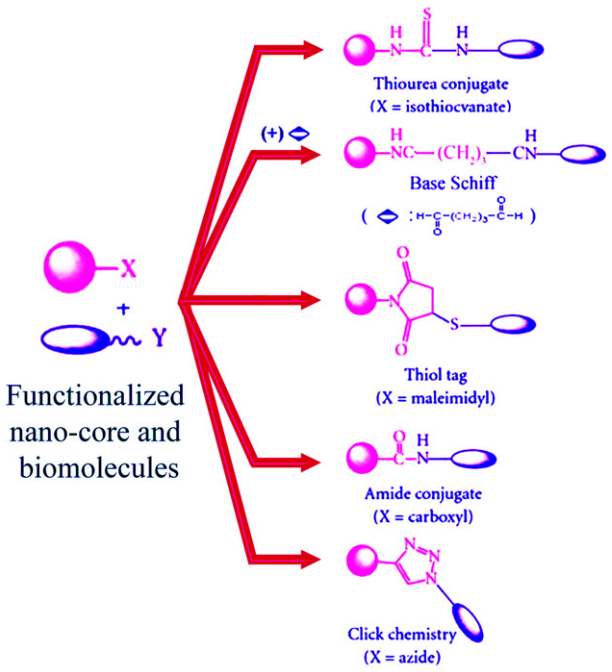

Figure 2. Bioconjugation routes based on chemical modification of nanostructures' surface with a biosystem to make a biosensor.

biolabel tool (biosensor) derived from the Eu(III) or Tb(III) lanthanide nanophosphors with 0D or 1D configuration. Furthermore, the LLN linked bioconjugate will be used as a biomedical label for recognizing virus/vaccine using fluorescence immunoassay (FIA). The first stage is synthesis of nanoparticles as $YVO_4:Eu(III)$ and Eu.NTA.TOPO complex and of nanorods $EuPO_4 \cdot H_2O$ and $TbPO_4 \cdot H_2O$ to matching fluorescent biomedical label tool. Then the binding of the lanthanide nanophosphors with an immunstimulative system such as immunoglobulin G (IgG) or bovine serum albumin (BSA) was investigated in the preparation of a new conjugate for biomedical application, in particular for fluorescent immunoassay analysis of virus or vaccine. In our work, the study was done by using a fluorescent optical microscope to detect and determine emission microplace on the surface of a specimen of the biomedical label expired vaccine. The results indicated that the bioconjugation method and LLN conjugate were effective and set the foundation for real application of lanthanide nanophosphors in research of viral biomedical process and potential application in quality control for industrial production of vaccine.

2. Experimental procedures

2.1. Synthesis of luminescent lanthanide nanomaterials

We have synthesized all the lanthanide nanophosphors in water for biomedical application. Nanosynthesis controlling the size, shape, structures and morphology was used thoroughly for lanthanide nanophosphors in the form of nanoparticles or nanorods [35]. Nanoparticle YVO_4: Eu(III) was synthesized by several techniques in an aqueous solution such as coprecipitation or in the presence of soft template [36,37]. Nanosized core/shell Eu.NTA.TOPO@PVP or silica was prepared with vortex technique in colloidal solvent system at room temperature [38]. Nanorods and wires $EuPO_4 \cdot H_2O$, $TbPO_4 \cdot H_2O$, $Eu_XTb_{1-X}PO_4 \cdot H_2O$ have been synthesized with assisted microwave heating in an opening reactor system [39,40].

2.2. Organic functionalization and binding of lanthanide nanophosphors with biomolecule

The functionalization of the nanophosphors is a key step toward biomedical application. As mentioned above, applications of nanoparticles require preliminary grafting at nanophosphor surface of organic or bio-organic functions. Different approaches are used such as encapsulation with functional polymers [41] or direct grafting of biofunctional ligands [42]. In this study, we used the approach that relies on the encapsulation of nanoparticles or nanorod with a thin layer of functional polysiloxane. They have been largely developed for the surface modification of various substrates such as flat silica or silicon wafer for adhesion promotion [24] or biochips [25]. Functionalization of colloidal nanoparticles has also been studied in many systems such as silica [43], magnetite [44] and quantum dot [45]. It has also been used in the case of lanthanide doped compounds such as gadolinium oxide [46] and lanthanum fluoride or ceriumphosphate [47,48].

In this study, the organic functionalization of $YVO_4:Eu(III)$, Eu.NTA.TOPO nanoparticles and $TbPO_4 \cdot H_2O$; $EuPO_4 \cdot H_2O$, $(Eu,Tb)PO_4 \cdot H_2O$ nanorods has used sol–gel technology. The first step is to build a protection shell for the nanophosphor core from the external microenvironment. In the meantime the protection shell provides improvement of the core stability, spectroscopic and physical properties. Besides, organic groups such as amine, mercapto, isothiocynate or carboxyl in the shell layer can be used for linking with biomolecule via a chemical reaction route. Shell materials bearing good biocompatibility will also improve the water emulsion stability, reduce unexpected immunophysiological side effects *in vivo*, and facilitate the penetration of nanophosphor core in biomedical environment.

2.2.1. Fabrication of the primary silicate shell as protect layer. 10 ml of methyltetraoxysililan and tetraethoxysililane (1/2) in absolute ethanol and 10 ml of as-synthesized $TbPO_4 \cdot H_2O$ solution was mixed by a magnetic stirring overnight at room temperature. The pH of this solution was adjusted to the range of 11–12 by adding NH_4OH 10 M. The resulting products were collected, centrifuged and washed several times with ethanol and distilled water. The final products were dried at 60 °C for 24 h in air.

2.2.2. Trialkoxysilane shell deposition. We have studied two trialkoxysilanes, aminopropyltrimetoxysililane (APTMS) or thiocyanate propyltrimetoxysililane (TCTMS) with NH_2 or SCN as functional groups. In typical synthesis, 22.5 ml of absolute ethanol and 2 ml of trialkoxysilane (either APTMS or TCTMS) were put in a 100 ml three-necked flask under magnetic stirring at room temperature for 30 min. The solution is heated up to 60 °C under reflux. Then 5 ml of the $TbPO_4 \cdot H_2O$ nanorod solution at pH 8 is added drop wise. The reaction time is about 3 h. The solution is then gently stirred for 20 h. The resulted products were collected

by three centrifugation/dispersion steps in a water/ethanol mixture (2:5, v/v). The final products were dried at 60 °C for 24 h in air.

2.2.3. Protein binding with sol–gel functionalized nanophosphors. Coupling of protein as immunoglobulin to the APTMS functionalized nanoparticles or nanorods was achieved using an amine reactive linker as glutaraldehyde or carbodimide [49, 50], or on the other hand to the thiocyanate by forming thioure linker [32, 51]. The APTMS treated $TbPO_4 \cdot H_2O$ nanorod solution and glutaraldehyde were dispersed in phosphate buffered saline (PBS, 0.1 M, pH 5) with concentration of $5\,g\,l^{-1}$. Immunoglobulin G (IgG) (Aldrich) of different concentration was added to 5 ml of the above solution. These reaction mixtures were incubated at 30 °C for 4 h. The resulting products were collected, centrifuged at 5900 rpm, and washed several times using ethanol and distilled water. The IgG linked $TbPO_4 \cdot H_2O$ nanorods were stored in closed box at 4 °C in a refrigerator.

2.3. Fluorescent immunoassay analysis

To demonstrate the application potential of IgG coupled LLNs in viral biology and medicine the investigation of the new nanolabel for detection of measles or rota viruses by using fluorescent immunoassay has been implemented. Vero cells of 3–4 days are detached by trypsin ethylendiaminetetraacetic acetic acid (EDTA) 0.05% solution making cell suspension at final concentration of 200,000 cell ml^{-1}. Add 3 ml-cell suspension/well (the coverslip was prior put in each well), incubate at 37 °C for three days in an incubator with 5% CO_2. Measles vaccine vial is reconstituted by 5.5 ml of distilled water and mixed well. Vaccine solution is diluted 10 times by minimum essential medium eagle (MEM) with 5% bovine serum, incubated 0.1 ml well (on cover slip vero cell), virus absorption at 37 °C, 60 min. Add 3 ml of MEM 2% bovine serum/well and incubate at 37 °C and 5% CO_2 for three days. Take out cover slip from the well and put in the tube with hole, inactivate the cell by acetone for 15 min, then wash 3 times by phosphate buffered saline (PBS). Dry the cover slip and set it on a slide glass. Put Ig-linked NP or NR on the surface of the cells. Close the tray and incubate at 37 °C for 60 min. Treat again with PBS 3 times. Dry the cover slip and then bring the specimen to imaging by a fluorescent optical microscopy for recognizing the virus.

2.4. Measuring equipment and measurements

The morphology of the as-synthesized samples was observed by using a field emission scanning electron microscopy (FE-SEM, Hitachi and S-4800). X-ray diffraction (XRD) measurements were performed on an x-ray diffractometer Siemens D5000 with $\lambda = 1.5406$ Å in the range of $15^{o} \leqslant 2\theta \leqslant 75^{\circ}$).

The photoluminescent (PL) spectra of the nanophosphors were also determined by using a spectrometer HORIBA JOBIN YVON IHR 550, NANOLOG iHR 320, HORIBA and conducted at room temperature. High-tech cleaning platforms for vaccine industrial production were used throughout the experimental cell incubation and FIA analysis. The microsized images of the specimens from the virus infected cells exposure with the conjugates from nanoparticles or nanorods have been viewed by a fluorescent microscopic equipment Olympus BX-40 (Japan) and pictured by a digital camera Nikon, D5000 with resolution of 12.30, f/3.5–5.6 G VR.

3. Results and discussion

3.1. The structures of the LLNs

3.1.1. $YVO_4 : Eu(III)$ nanoparticles [52]. The mean size of the YVO_4 : Eu(III) nanoparticles at 160–180 °C prepared by using the hydrothermal technique is about 18–20 nm. As temperature increases 200–220 °C, the mean size decreases to around 10 nm. When increasing the reaction time from 1 to 24 h, the particle size is reduced from 12 to 8 nm and distributed more evenly. Thus, with the factors of temperature and reaction time, we can control the desired nanoparticles size. Most of the nanoparticles reported in past immunoassays are from 30 to 20 nm in diameter. Particle sizes over 30 nm are proven to bring obviously prolonged equilibration time and enhanced nonspecific adsorption [24]. The nanoparticles with smaller sizes have improved kinetic properties and non-specific adsorption. Moreover, the nanoparticles should be big enough to bind several proteins on the surface, which is expected to increase the immunological affinity [50]. The XRD pattern of the YVO_4 : Eu(III) nanoparticles is investigated in detail. The crystal form of the obtained YVO_4 : Eu(III) nanoparticles is wakefieldite (Y) tetragonal.

3.1.2. Eu_XTb_{1-X}.NTA.TOPO [38]. In this research uniform fluorescent nanoparticles were synthesized in one step at room temperature. From the FESEM images of synthesized nanoparticles of Tb(III) doped Eu(III) chelate with TOPO and NTA ligands, aggregation of nanoparticles is not observed. The obtained nanosized particles were uniform with a mean diameter of 25 ± 5 nm and shell thickness of 10 nm.

The Fourier transform infrared (FTIR) spectra of the synthesized nanoparticles of Tb(III)-doped Eu(III) chelates showing a broad band at wavenumber of $3444\,cm^{-1}$ is attributed to the H_2O molecule, and the band at $1650\,cm^{-1}$ related to the C = O group of the ligand. The complexation between Eu(III) and Tb(III) with NTA.TOPO ligands is evidenced by a narrow band located at $1388\,cm^{-1}$, which appeared to prove that Eu(III) or Tb(III) ions may be coordinated to two oxygen atoms of ligands.

The successful synthesis of a nanosized metalorganic complex having the active rare earth mixing ions Tb and Eu with high quantum yield emission, high photostability and their good water solubility provides promising research for biomedical photonic engineering.

3.1.3. $EuPO_4 \cdot H_2O$ nanorods [37], $TbPO_4 \cdot H_2O$ *[36, 39] and* Eu_XTb_{1-X} $PO_4 \cdot H_2O$ *nanorods and nanowires [40].* From the FE-SEM images, one can estimated that the mean size of the $EuPO_4 \cdot H_2O$ nanorods is about 15–20 nm in diameter and 300–500 nm in length. For the case of the $EuPO_4 \cdot H_2O$ nanorods prepared by using diethylene

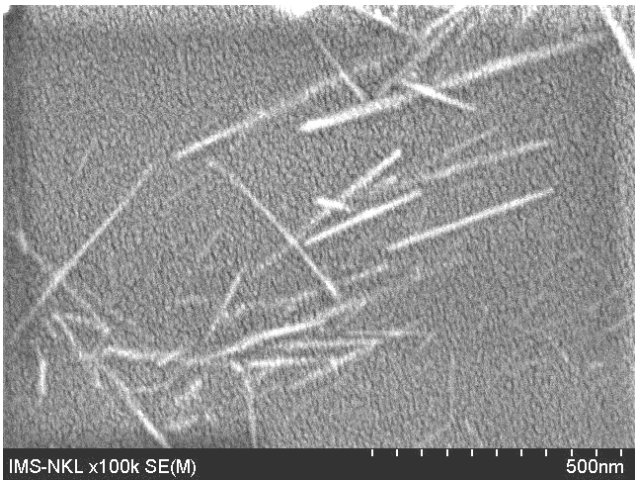

Figure 3. FE-SEM of $TbPO_4 \cdot H_2O$ nanorods/nanowires, MW power <500 W.

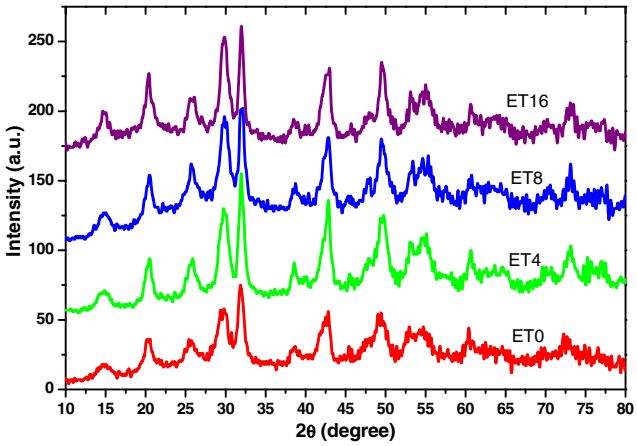

Figure 4. XRD patterns of $Eu_XTb_{1-X}PO_4 \cdot H_2O$ nanorod synthesized by using MW heating with different Eu^{3+}/Tb^{3+} molar ratios. ET16- code: $Eu_{0.0625}Tb_{0.9375}PO_4 \cdot H_2O$; ET18-code: $Eu_{0.0555}Tb_{0.9445}PO_4 \cdot H_2O$; ET4-code: $Eu_{0.2500}Tb_{0.7500}PO_4 \cdot H_2O$; ET0-code: $TbPO_4 \cdot H_2O$.

glycol (DEG), the length of $EuPO_4 \cdot H_2O$ nanorods became shorter with 100–300 nm, while the diameter is almost the same. Similarly, by using polyethylene glycol (PEG) in the preparative procedure of $EuPO_4 \cdot H_2O$ nanorods, the mean sizes of $EuPO_4 \cdot H_2O$ nanorods are about 15–20 nm in diameter and 200–300 nm in length. Therefore, with results of FE-SEM, a pivotal role of soft template agents in reducing the nanorods' mean length was clarified.

The $EuPO_4 \cdot H_2O$ prepared at pH = 2 indicates that the nanorods have bundle shapes with the lengths of rod about 300–500 nm and diameter of rod about 15–20 nm. With the increase in pH value to pH = 6 or pH = 8, the length of nanorods was decreased to about 150–250 nm while the diameter of nanorods was unchanged.

The prepared $EuPO_4 \cdot H_2O$ nanorods showed a rhabdophane-type hexagonal form. Qualitatively, the use of DEG and PEG as soft template agents causes no change in crystalline phase composition.

The hydrated europium orthophosphate was always obtained as a unique product. It is a real perspective result with regard to biological fluorescence labeling application, which required luminescent nanomaterials to react with biological species readily [29].

The FE-SEM images of $TbPO_4 \cdot H_2O$ samples synthesized by using microwave (MW) heating of an aqueous solution containing $Tb(NO_3)_3$ and $NH_4H_2PO_4$ at pH = 2 with various microwave irradiated powers ranged from 300 to 900 W were studied. The nanorods/nanowires are uniformly distributed with diameters in the range of 5–10 nm and lengths ranged from 150 to 350 nm (figure 3). There exists a critical value of irradiated power of 500 W for these nanorods/nanowires tending to bunch with the further increase in microwave irradiated powers.

XRD patterns of the as-synthesized $TbPO_4 \cdot H_2O$ nanorods/nanowires indicate only single crystalline phase of $TbPO_4 \cdot H_2O$. All diffraction peaks can be distinctly indexed to a rhabdophane-type pure hexagonal phase. These results are as similar as those reported previously [12]. Qualitatively, the switching of microwave irradiated power causes no change in chemical composition as well as crystalline phase. This implied that, by using microwave synthesis apparatus and an aqueous solution containing $Tb(NO_3)_3$ and $NH_4H_2PO_4$ at suitable reaction conditions on pH value, the hydrated terbium orthophosphate, was always obtained as a unique product instead of anhydrous $TbPO_4$. In the crystal structure of this monohydrate salt, each Tb^{3+} cation is not coordinated by oxygen atoms which reside at two different crystallographic sites, O1 and O2, of PO_4^{3-} anions only as observed in the case of $TbPO_4$, but is also connected to oxygen atoms (O3w) of two hydrate water molecules. The interatomic distances between Tb^{3+} cation and oxygen atoms of two hydrate water molecules of about 2.6 Å are significantly longer than those of Tb^{3+} cation and oxygen atoms of PO_4^{3-} anions (about 2.3 Å).

As a result, it is quite reasonable to expect that $TbPO_4 \cdot H_2O$ nanomaterials exhibit higher hydrophilability and are better distributed in water medium than those of anhydrous $TbPO_4$. Indeed these material features of $TbPO_4 \cdot H_2O$ nanorod enable more chemical activity and also more compatibility with a biomedical system. It is really a perspective result regarding biomedical labeling, which requires high hydrophilability and biocompatibility of luminescent nanomaterials.

In our laboratory for the first time $Eu_X, Tb_{1-X}PO_4 \cdot H_2O$ nanorods and nanowires with lengths from 150–200 nm and widths of about 5–6 nm were successfully synthesized with various concentration rates (X) of Eu and Tb by using different MW power. The decrease in Eu^{3+} molar concentration led to the increase in length of nanorods/nanowires from 150 to 300 nm and, at the same time, the increase in their width from 5 to 10 nm. $(Eu,Tb)PO_4 \cdot H_2O$ nanorods/nanowires indicate only single crystalline phase. All reflections of the XRD patterns can be distinctly indexed to a rhabdophane-type pure hexagonal phase (figure 4).

This implies that the crystal structures of all Eu^{3+}-doped terbium orthophosphate monohydrates are isostructural to that of pure $TbPO_4 \cdot H_2O$.

Thus, by using microwave synthesis method and an aqueous solution containing nitrates of trivalent rare-earth ions and $NH_4H_2PO_4$ at a suitable pH value of 2 the hexagonal phase of europium/terbium orthophosphate monohydrate

(Eu,Tb)$PO_4 \cdot H_2O$, was obtained as a unique product with Eu(III) molar concentration ranging from 6 up to 20 at.%.

3.2. The photoluminescence properties

3.2.1. YVO_4 : Eu(III) nanoparticles [52]. YVO_4 : Eu(III) nanoparticles exhibit strong red luminescence with narrow bands corresponding to the intra-4f transitions of $^5D_0$–^7F_j ($j = 1, 2, 3, 4$) Eu^{3+}. The peaks were found at 594 nm ($^5D_0$–$^7F_1$), 619 nm ($^5D_0$–$^7F_2$), 651 nm ($^5D_0$–$^7F_3$), and 697 nm ($^5D_4$–$^7F_4$), with the strongest emission at 619 nm. The emission peak at 619 nm of europium ions was split into two sharp peaks at 615 and 619 nm because of the change of ligand field of Eu^{3+}.

3.2.2. Nanosized Eu.NTA.TOPO chelates [38]. Emission spectra of nanostructured Eu(III) chelates and Tb(III)-doped Eu(III) chelates in aqueous solution were measured under excitation of $\lambda_{exc} = 325$ nm and $\lambda_{exc} = 370$ nm. It can be seen that the nanoparticle complexes exhibit the characteristic narrow emission peaks at 616 nm of trivalent lanthanide ions. The emission spectra consist of four main peaks at 593, 616, 652 and 702 nm, which correspond to the $^5D_0 \rightarrow ^7F_n$ ($n = 1, 2, 3, 4$) transitions of Eu($^5D_0 \rightarrow ^7F_1$ at 593 nm, $^5D_0 \rightarrow ^7F_2$ at 616 nm, $^5D_0 \rightarrow ^7F_3$ at 652 nm and $^5D_0 \rightarrow ^7F_4$ at 702 nm).

The influence of the dopant to optical properties of the nanoparticle complexes of Tb(III)-doped Eu(III) was investigated. The shape of the spectra of Tb(III)-doped Eu(III) chelate nanoparticles is similar to that of Eu(III) nanoparticles and the emission maximum is not shifted. However, the fluorescent intensity of nanoparticles in aqueous solution depends strongly on the ratio of Tb(III) in Eu(III) chelates.

3.2.3. $EuPO_4 \cdot H_2O$ nanorods [37], $TbPO_4 \cdot H_2O$ [36,39] and $Eu_XTb_{1-X}PO_4 \cdot H_2O$ nanorods/nanowires [40]. A photoluminescence excitation spectrum of the $EuPO_4 \cdot H_2O$ nanorods can either be optically excited in the UV region or in the visible one. The excitation wavelengths of the $EuPO_4 \cdot H_2O$ nanorods were 317, 361, 375, 393, 414 and 464 nm. The excitation of $EuPO_4 \cdot H_2O$ nanorods at any of these wavelengths resulted in similar emission spectra in the red spectral region.

The main emission peaks for $EuPO_4 \cdot H_2O$ nanorods were observed at 594, 619, 652 and 697 nm (due to the $^5D_0$–$^7F_1$, $^5D_0$–$^7F_2$, $^5D_0$–$^7F_3$ and $^5D_0$–$^7F_4$ transitions of Eu(III), respectively) under excitation at 393 or 464 nm. $EuPO_4 \cdot H_2O$ nanorods yielded the characteristic emission of Eu(III), in which the magnetic dipole allowed $^5D_0$–$^7F_1$ transition at 594 nm is the most prominent emission line. This transition is stronger than the electric dipole allowed $^5D_0$–$^7F_2$ transition of Eu^{3+} due to the higher symmetry of active ion. Nevertheless, in all the fluorescence spectra of $EuPO_4 \cdot H_2O$ only a small nib at 578 nm has been found, which can be assigned to $^5D_0$–$^7F_0$ transition.

In photoluminescence excitation spectra of $TbPO_4 \cdot H_2O$ nanorods/nanowires monitored at 542 nm emission line there were the bands of 310, 350, 370 and 480 nm. The peak in photoluminescence excitation spectra at 480 nm is due to the spin allowed $^7F_6$–$^5D_4$ transition of the Tb(III) ions. The other peaks at 350–370 and 310 nm are assigned to the intra $4f^8$ transitions between the $^7F_6$–$^5L_{10-7}$ and $^7F_6$–$^5H_{7-4}$, respectively. It can be concluded that the excitation spectra of $TbPO_4 \cdot H_2O$ nanorods/nanowires arise from the optical transitions of trivalent terbium ion Tb(III).

The photoluminescence spectra under 370 nm excitation of $TbPO_4 \cdot H_2O$ nanowires synthesized by using different irradiated powers have the emission intensity varied as a function of irradiated power and reached a maximum value with 500 W. For $TbPO_4 \cdot H_2O$ nanorods/nanowires, the emission bands centered at 488, 542, 584 and 620 nm are assigned to $^5D_4 \rightarrow ^7F_J$ transitions ($J = 6$, 5, 4, 3), respectively. The maximum emission peak is found at 542 nm of wavelength corresponding to $^5D_4$–$^7F_5$ transition.

The photoluminescence spectra of $Eu_XTb_{1-X}PO_4 \cdot H_2O$ nanorods/nanowires of all investigated Eu(III)/Tb(III) molar ratios were recorded under 370 nm excitation. The intensity of four emission peaks found at 589, 615, 650 and 695 nm varied as a function of the Eu(III)/Tb(III) molar ratio and reached a maximum value with the Eu^{3+}/Tb^{3+} molar ratio of 1/8. This originated from the energy transfer from Tb(III) to Eu(III) ions due to the energy overlap between the donor Tb(III) and the acceptor Eu(III).

The emission spectra with characteristic red emission of Eu(III) ions corresponding to the transitions from $^5D_0$ to the ground states ^7F_j ($j = 1$, 2, 3, 4) are observed, respectively. It is quite interesting that the strongest energy transfer from Tb(III) to Eu(III) ions was found with the Eu^{3+} molar concentration of about 11%. This value is significantly higher than that reported in previous works (about 5 at.%) [53]. For all samples containing Tb(III) ions, the characteristic fluorescence emission peak of 543 nm was observed. The intensity of this peak, however, was suppressed with the increase of Eu^{3+} incorporated into the host lattice due to the inhibition of spontaneous emission [54]. The strong enhancement in intensity of four emission peaks of $Eu_{0.125}Tb_{0.875}PO_4 \cdot H_2O$ sample at 589, 615, 650 and 695 nm with respect to that of the pure $EuPO_4 \cdot H_2O$ sample confirms once again the existence of the energy transfer in (Eu,Tb)$PO_4 \cdot H_2O$ nanorods/nanowires.

3.3. Organic functionalization and bioconjugation

The conditions used for silica deposition were chosen to optimize the functional group on the surface for the lowest possible thickness and also to keep the emission properties unchanged.

We present here the influence of the shells and organic functionalization on the photoluminescent characterization of some typical Ln-nanophosphors, for instance, in $TbPO_4 \cdot H_2O$ nanorod.

Surface defects also play important roles in quenching the luminescence of nanophosphor due to the large surface-to-volume ratio of nanophosphors.

Based on experimental and theoretical studies, many reports have confirmed that surface and interior environments are different for Ln-ions doped in nanophosphors (figure 5(a)). The situation was substantially changed when the nanophosphor is coated with a functional group linked shell such as amine (NH_2) or thiocyanate (SCN) (figures 5(b) and (6)). The decreasing fluorescence intensities of coated

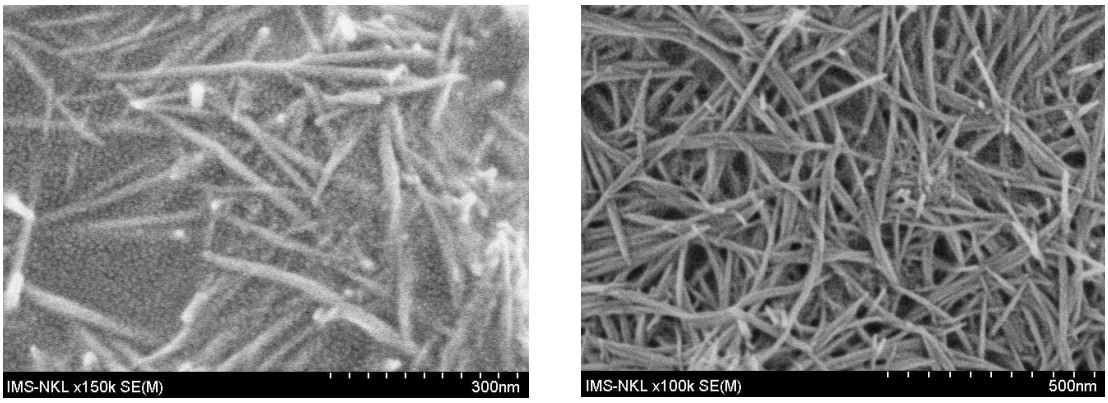

(a) **(b)**

Figure 5. FESEM of $TbPO_4 \cdot H_2O$ nanorod@Silica (a) and $TbPO_4 \cdot H_2O$ nanorod@Silica-NCS (b).

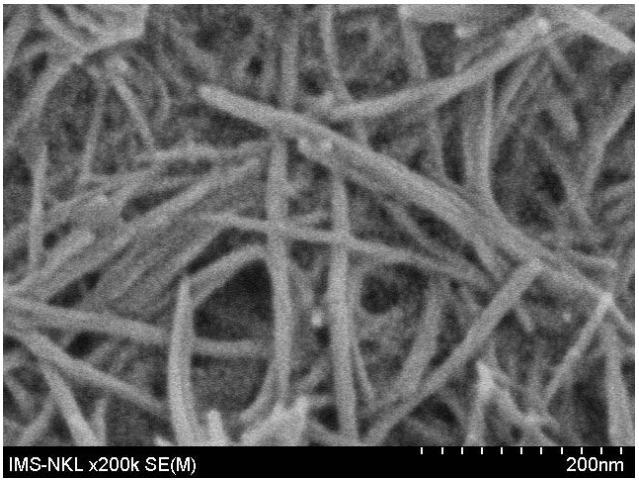

Figure 6. FESEM of $TbPO_4 \cdot H_2O$ -nanorod@Silica-(NCS) $\leftrightarrow$ IgG.

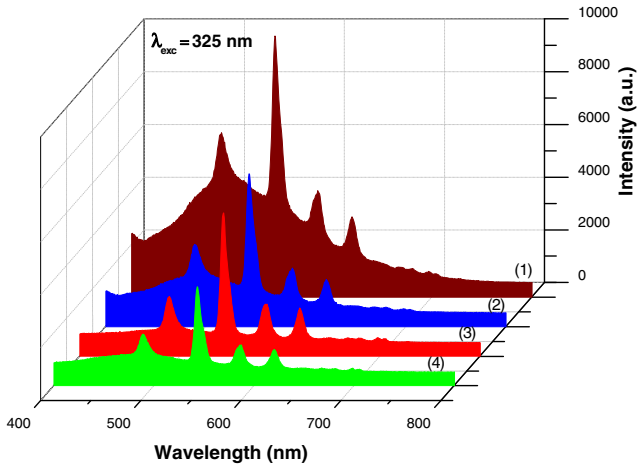

Figure 7. Photoluminescence spectra of $TbPO_4 \cdot H_2O$ (1); $TbPO_4 \cdot H_2O$@Silica (2); $TbPO_4 \cdot H_2O$@Silica-NCS (3) and $TbPO_4 \cdot H_2O$@Silica-NCS $\leftrightarrow$ IgG (4). λ_{exc} at 325 nm.

nanophosphors $TbPO_4 \cdot H_2O$ (1), $TbPO_4 \cdot H_2O$@Silica (2), $TbPO_4 \cdot H_2O$@Silica-NCS (3) and $TbPO_4 \cdot H_2O$ @Silica-NCS $\leftrightarrow$ IgG (4) are presented in figure 7. It is noted that the organic groups NH_2 or SCN are rather strong dipole. In this case they may strongly attack core surface to reduce the luminescence.

To develop a new conjugate being suitable for labeling we focused on some strong bioaffinity molecules and organisms such as biotin, protein immunoglobulin G (IgG) or bovine serum albumin (BSA).

Based on the immunoreactions between antibody of conjugate and antigen of virus/vaccine the products of immunoreactions can be detected by a fluorescence optical microscope and imaged by a digital camera. In this study, we have used two coupling reaction processes to build a conjugate. They consisted of forming thiourea from isothiocyanate and amine and linking this functional group with biomolecule via intermediate glutaraldehyde molecule. With the obtained conjugates using IgG as targeting biomolecule we have demonstrated the analysis of measles or rota vaccines which are the key products of the Industrial Centre for Investigation and Production of Vaccine and Biologicals (POLYVAC).

3.4. Application in fluorescent immunoassay (FIA) of viruses/vaccine

We applied the comparative analysis method and used the conjugate of Ig-linked nanoparticles or nanorod as well as the commercial conjugate (for the reference) in the cell incubation procedure of POLYVAC for vaccine production. We have experimentally researched different conjugated materials in two forms of nanoparticle or nanorod such as IgG-YVO_4 : Eu(III)-NP, Eu.NTA.TOPO-NP, $TbPO_4 \cdot H_2O$-NR, $EuPO_4 \cdot H_2O$-NP and (Eu, Tb)$PO_4 \cdot H_2O$-NR in incubation process with vaccine fabricates.

The images for reference obtained from fluorescent microscopic measurements and cameras pictured are shown in figure 8. In figure 8(a), one can see the picture of the fluorescent microscope BX-40 equipment (Japan), and the images of the specimen surface of incubated Vero cells as standard raw cells for vaccine fabrication are in figure 8(b). Figure 8(c), shows the images of Vero cells (figure 8 (c)) and infected with measles virus, both researched specimens used a commercial conjugate as reference.

Figure 9 showed the potential application of LLNs linked with IgG as a fluorescence immunolabel to measles vaccine. The incubation procedure with exposure of the

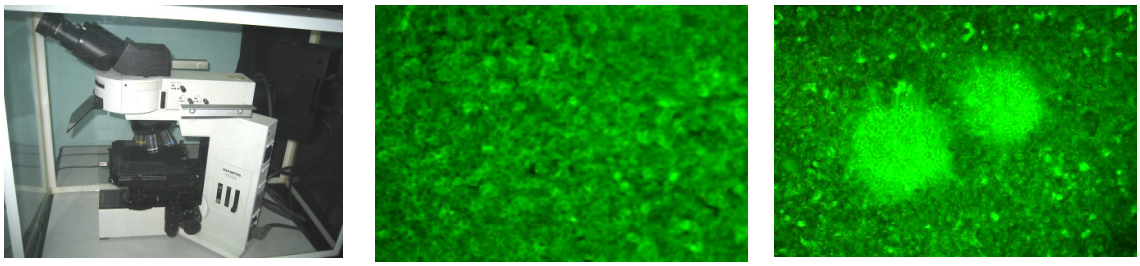

(a) **(b)** **(c)**

Figure 8. Fluorescent microscope Olympus BX-40 (Japan) (a), Vero cells (b) and Vero cell infected with measles virus (c).

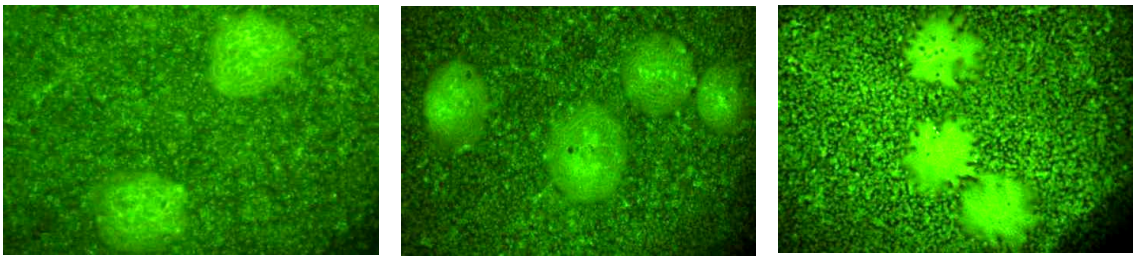

(a) **(b)** **(c)**

Figure 9. Micro-image of measles virus infected Vero cells using $TbPO_4$-IgG code: 020911 (a) (Tb, Eu)PO_4-IgG code: 030911 (b) and $EuPO_4$-GDA-IgG code: 040911 (c).

conjugate was used for preparing the measured specimens. The micro-image of the specimens with measles virus infected Vero cells using $TbPO_4$-IgG code: 020911 (figure 9(a)), (Tb,Eu)PO_4-IgG code: 030911 (figure 9(b)), $EuPO_4$-GD-IgG code: 040911(figure 9(c)) as fluorescent immunoassay probe were presented.

The results indicated that some fabricated conjugates could be well used for detection and viewing of the presence of measles vaccine and quality of the fabrication. In comparison with nanoparticle derived biolabels, the LLN conjugates based on nanorods or nanowires have been shown to be much more effective. The reason for this may be explained by the stronger internalization effect of anisotropic properties of nanorods to biocells [12]. Primarily it can be stated that Ig-$TbPO_4 \cdot H_2O$-NR, IgG-$EuPO_4 \cdot H_2O$-NR and IgG-(Eu,Tb)$PO_4 \cdot H_2O$-NR are usable for the FIA analysis method. The properties of fluorescence microscopic images clearly enabled estimation of measles vaccine containing big clusters on the surface of the specimens. The quality of the investigated lanthanide conjugates for FIA analysis could be comparable with the used reference label. Nevertheless, the prepared lanthanide conjugates have shown a high stable fluorescence color and reproducible fluorescent intensity in a broad range of pH value, and in biological microenvironment of vaccine fabrication. The fluorescence properties of the assayed specimens clearly remained for several months.

4. Conclusion

In conclusion, it was demonstrated that high luminescent nanoparticles and nanorods from $YVO_4 : Eu(III)$, EuNTA.TOPO, $TbPO_4 \cdot H_2O$, $EuPO_4 \cdot H_2O$ and (Tb,Eu)$PO_4 \cdot H_2O$ have been prepared by coprecipitation synthesis in aqueous medium, with the assistance of microwave and a soft template. These nanophosphors with controlled size, shape and structures were coated with organic silica toward functionalizing with organic groups NH_2, SH, SCN and OH. Then SCN- or NH_2-containing silica layers on nanophosphor surface were covalently coupled with biotin, IgG or BSA via coupling reaction. Based on the application results it has been stated that the procedure consisting of the virus infected standard cell incubation protocol and the exposure with IgG-linked LLN conjugates were provided with a new fluorescent label tool for FIA analysis of virus in diagnosis or in vaccine production. In comparison with nanoparticle derived biolabels the LLN label tools from nanorods or nanowires have shown to be much more effective. Furthermore, the IgG (BSA)-linked LLN-conjugates may have wide application in biolabel and bioimaging of bioorganisms such as protein, cells and virus, and also for technological development of vaccine industrial production. Besides, these LLN conjugates will be used for the development of novel diagnostic tools in biomedicine and agriculture. However, much work still needs to be done before these LLN conjugates become a useful and ordinary biophotonic label or sensor in practical application.

Acknowledgments

This work was supported by Vietnam Ministry Science and Technology, project no 2–2–742/ DTDLNN 09–12 and partly NAFOSTED foundation, projects no. 103.06.46.09 included and implementing in Institute of Materials Science (IMS), in Key laboratory of Electronic Materials and Devices, Vietnam Academy of Science and Technology, in long term and close collaboration with Center of Research and Production of Vaccine and Biologicals (POLYVAC), in framework of joint project of basic research for development of fabrication

technology no 05/2009–09–12. We thank Professor Wieslaw Strek (Poland), Professor Chia Chen Hsu (Taiwan) and Professor Tamio Endo (Japan) for international cooperation. We are grateful for the encouragement and continuous support of Professor Acad. Nguyen Van Hieu (Vietnam).

References

[1] Slata O V 2004 *J. Nanobiotechnol.* **2** 3
[2] Wang F, Tan W B, Zhang Y, Fan X and Wang M 2006 *Nanotechnology* **17** R1
[3] Liu Z, Kiesling F and Gaetjens J 2010 *J. Nanomater.* Article ID894303
[4] Kanngangai R, Abraham A M, Sanker S and Sridharan G 2010 *J. Med. Microbiol.* **28** 95
[5] Manchester M and Steinmetz N F (ed) 2010 *Viruses and Nanotechnology* (Heidelberg: Springer)
[6] Yalow R S and Benson S A 1959 *Nature* **184** 1648
[7] Holmes KL and Lantz LM 2001 *Methods Cell Biol.* **63** 185
[8] Kirchner C, Liedl T, Kudera S, Pellegrino T, Javier A M, Gaub H E, Stölzle S, Fertig N and Parak J W 2005 *Nanoletter* **5** 331
[9] Stowdam J W and van Veggel F 2004 *Langmuir* **20** 11763
[10] Rokowski K and Haase M 2003 *J. Phys. Chem.* B **102** 10129
[11] Kömpe K, Borchert H, Storz J, Lobo A, Adam S, Möller T and Haase M 2003 *Angew. Chem. Int. Engl.* **42** 5513
[12] Patta C R, Bhattacharya R, Pattra S, Basu S, Mukherjee P and Mukhopadhyay D 2006 *J. Nanobiotechnol.* **4** 11
[13] Wong K-L, Law G-L, Murphy M B, Tanner P A, Wong W-T, Lam P K-S and Lam M H-W 2008 *Inorg. Chem.* **47** 5190
[14] Liu G and Chen X 2007 *Handbook of the Physics and Chemistry of Rare Earth, Optical Spectroscopy*, vol 37 (Amsterdam: North-Holland) chapter 233, pp 99–169
[15] Minh L Q, Strek W, Anh T K and Yu K (Guest ed) 2007. *Nanomater. Lumin. Nanomater.* 2007 (Special issue) ID43812
[16] Stouwdam J W, Hebbink G A, Huskens J, Van V and Frank C J M 2003 *Chem. Mater.* **15** 4604
[17] Meyssamy H, Riwotzki K, Kornowski A, Naused S and Haase M 2004 *Adv. Mater.* **11** 16697
[18] Wu C, Qin W, Qin G, Zhao D, Zhang J, Huang S, Lu S, Liu H and Lin H 2003 *Appl. Phys. Lett.* **82** 520
[19] Wu X, Tao Y, Song C, Mao C, Dong L and Zhu J 2006 *J. Phys. Chem.* B **110** 15791
[20] Duan X, Yang Y, Cui Y, Wang J and Lieber C 2001 *Nature* **409** 66
[21] Pan Z, Dai Z and Wang Z 2001 *Science* **291** 1947
[22] Hreniak D, Doskocz J, Gluchowski P, Lisiecki R, Strek W, Vu N, Loc D X, Anh T K, Bettinelli M and Speghinia A 2011 *J. Lumin.* **131** 473
[23] Law G L, Wong K L, Kwok W M, Wong W T and Tanner P A 2007 *J. Phys. Chem.* B **111** 1058
[24] Soulka T, Paukkunen J, Haermae J, Lönnberg S, Lindroos H and Lövgren T 2001 *Clin. Chem.* **47** 1269
[25] Harma H, Graf C and Hannienen P 2008 *J. Nanopart. Res.* **10** 1224
[26] Li M and Selvin P R 1997 *Bioconjug. Chem.* **8** 127
[27] Wang F and Liu X 2009 *Chem. Soc. Rev.* **38** 976
[28] Li Z, Zhanf Y and Jiang S 2008 *Adv. Mater.* **20** 4765
[29] Park Y I *et al* 2009 *Adv. Mater.* **21** 4467
[30] Xiong L Q, Chen Z G, Yu M X, Li F Y, Liu C and Huang C H 2009 *Biomaterials* **30** 5592
[31] Lam T K G, Opalinska A, Chudoba T, Benkowski K, Lojkowski W, Tran K A, Nguyen T B and Le Q M 2010 *Adv. Nature Sci., Nanosci. Nanotechnol.* **1** 025008
[32] Hermanson G T 2008 *Bioconjugate Techniques* 2nd edn (New York: Elsevier)
[33] Roy I, Ohulchanskyy T Y, Bharali D J, Pudavar H E, Mistretta R A, Kaur N and Prasad P N 2005 *Proc. Natl Acad. Sci. USA* **102** 279
[34] Zhu S G *et al* 2004 *Biotechnol. Appl. Biochem.* **39** 179
[35] Minh L Q, Endo T, Huong T T, Huong N T, Giang L T K, Tuyen L D, Loc D X and Anh T K 2010 *Trans. MRS Japan* **35** 417
[36] Huong T T, Anh T K, Khuyen H T, Hien P T and Minh L Q 2012 *Adv. Nature Sci., Nanosci. Nanotechnol.* **3** 015010
[37] Huong T T, Anh T K, Vinh L T, Strek W, Khuyen H T and Minh L Q 2011 *J. Rare Earths* **29** 1174
[38] Khuyen H T, Huong N T, Huong T T, Anh T K, Binh N T and Minh Le L Q 2011 *Adv. Nature Sci., Nanosci. Nanotechnol.* **2** 025015
[39] Huong N T, Khuyen H T, Duc Van N, Tien D M, Binh N T and Minh L Q 2012 *Adv. Nature. Sci., Nanosci. Nanotechnol.* **3** 015007
[40] Huong N T, Duc Van N, Tien D M, Tung D K, Binh N T, Anh T K and Minh L Q 2011 *J. Rare Earths* **29** 1170
[41] Mornet S, Vasseur S, Grasser F and Dugnet E 2004 *J. Mater. Chem.* **14** 2161
[42] Traina C and Schwartz A 2007 *Langmuir* **23** 9158
[43] Howarter J A and Youngblood J P 2006 *Langmuir* **22** 11142
[44] Flesch C, Robert M, Bourgeay-Lami E, Mornet S, Duguet E, Delaire C and Durmas P 2005 *Colloids Surf.* A **262** 150
[45] Douce J, Boilot J-P, Biteau J, Scodellaro L and Jimenez A 2004 *Thin Solid Films* **466** 114
[46] Philipse A P, Nechifor A-M and Patmamanoharan C 1994 *Langmuir* **10** 4451
[47] Gerion D, Pinaud F, Williams S C, Parak W J, Zancher D, Wriss S and Alivisatos A P 2001 *J. Phys. Chem.* **105** 8861
[48] Loc D X, Chi T K, Huong T T, Vu N, Anh T K, Strek W and Minh L Q 2011 *J. Rare Earths* **29** 1174
[49] Louis C, Bazzi R, Marquette C A, Bridot J-L, Roux S, Ledoux G, Mercier B, Blum L, Perriat P and Tillement O 2005 *Chem. Mater.* **17** 1673
[50] Sivakumar S, Diamente P R and Van Veggel F C J M 2006 *Chem.—Eur. J.* **12** 5878
[51] Kang J, Zhang X Y, Sun L D and Zhang X X 2007 *Talanta* **71** 1186
[52] Huong T T, Tu V D, Anh T K, Vinh L T and Minh L Q 2011 *J. Rare Earths* **29** 1137
[53] Di W, Wang X, Zhu P and Chen B 2007 *J. Solid State Chem.* **180** 467
[54] Yang Z, Huang X, Sun L, Zhou J, Yang G, Li B and Yu C 2009 *J. Appl. Phys.* **105** 083523